Journal of Fluorescence, Vol. 16, No. 1, January 2006 (© 2006)
DOI: 10.1007/s10895-005-0024-1

Intensity Range Based Quantitative FRET Data Analysis to Localize Protein Molecules in Live Cell Nuclei

Ye Chen[1] and Ammasi Periasamy[1,2,3]

Received July 18, 2005; accepted October 14, 2005
Published online: January 6, 2006

Förster (fluorescence) resonance energy transfer (FRET) is an ideal technique to estimate the distance between interacting protein molecules in live specimens using intensity-based microscopy. The spectral overlap of donor and acceptor— essential for FRET—also generates a contamination of the FRET signal. There are a number of algorithms available to remove this spectral bleedthrough (SBT) contamination and in this paper we compare two popular algorithms to estimate the SBT element and to calculate a more precise level of energy transfer efficiency, and with that a more accurate distance estimate.

KEY WORDS: FRET; spectral bleedthrough (SBT); protein–protein interactions; green fluorescent proteins (GFPs).

INTRODUCTION

Förster (fluorescence) resonance energy transfer (FRET) is a widely used technique to measure the distance between two molecules which are labeled with two different fluorophores (donor and acceptor) [1–4]. While the basic technique is relatively straightforward, there are a number of important considerations—discussed later—to calculate a reliable level of energy transfer efficiency ($E\%$), which is the basis for a more precise distance estimate between interacting molecules, free from artifacts and signal contaminations.

There are a number of methodologies used to study the protein–protein interactions including affinity chromatography, co-immunoprecipitation, non-denaturing electrophoresis, covalent cross-linking, X-ray diffraction, electron microscopy, and spectroscopic methods [5]. These methods do not provide direct access to the interactions of protein partners in their natural environment. On the other hand, an intensity-based FRET microscopy imaging technique facilitates these studies in intact subcellular components and provides two- or three-dimensional distribution of protein associations under physiological condition [6–10].

FRET is a process involving the radiationless transfer of energy from a donor fluorophore to an appropriately positioned acceptor fluorophore [2,3,11]. FRET can occur when the emission spectrum of a donor fluorophore significantly overlaps (>30%) the absorption spectrum of an acceptor (Fig. 1), provided dipoles of the donor and acceptor fluorophores are in favorable mutual orientation. Because the efficiency of energy transfer varies inversely with the sixth power of the distance separating the donor and acceptor fluorophores, the distance over which FRET can occur is limited to between 1–10 nm. When the spectral, dipole orientation, and distance criteria are satisfied, excitation of the donor fluorophore results in sensitized fluorescence emission from the acceptor, indicating that the tagged proteins are separated by <10 nm.

Advances in optics, digital computers, digitizers and image processing software and low light level photodetectors have improved the application of FRET microscopy [7,12]. The development of mutant forms of green

[1] W.M. Keck Center for Cellular Imaging, University of Virginia, Gilmer Hall, Charlottesville, Virginia 22904.
[2] Departments of Biology and Biomedical Engineering, University of Virginia, Gilmer Hall, Charlottesville, Virginia 22904.
[3] To whom correspondence should be addressed. E-mail: ap3t@virginia.edu.

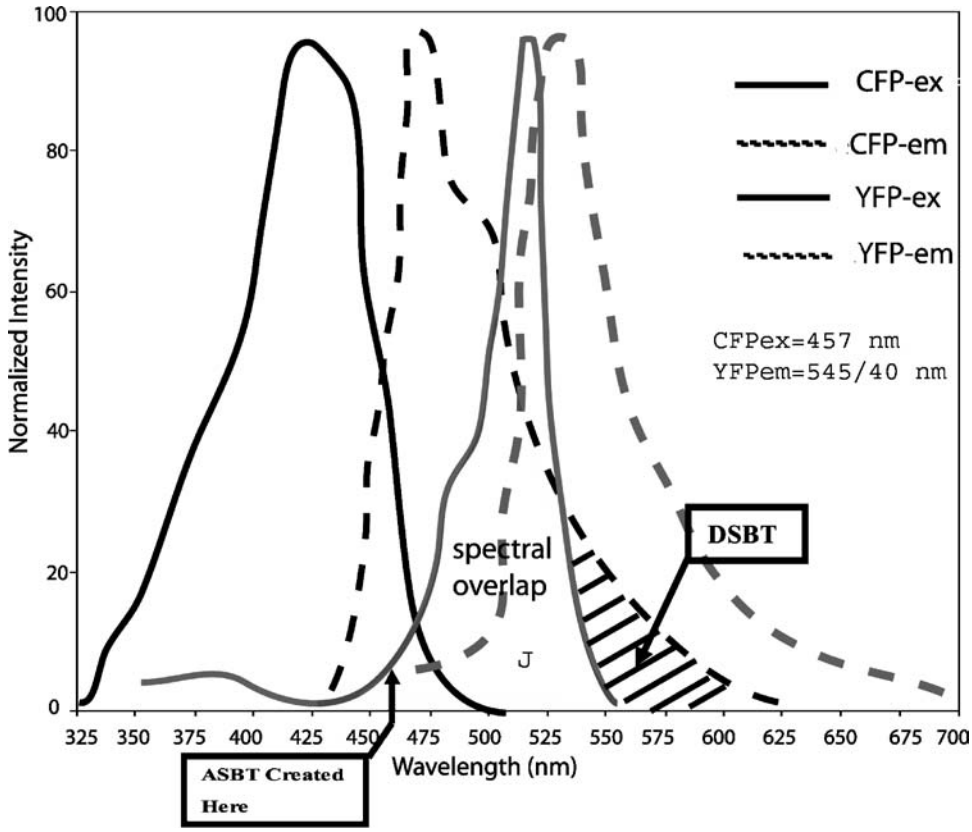

Fig. 1. Absorption and emission spectra of eCFP and eYFP. The DSBT area in the eYFP emission channel represents the donor spectral bleedthrough in the FRET channel and the arrow shows the donor excitation wavelength (457 nm) exciting acceptor molecule to cause acceptor bleedthrough.

fluorescent proteins (GFPs), which can be used to reveal the chemical and molecular dynamics of proteins in intact cells, has significantly broadened the usefulness of FRET microscopy, allowing localization and measurement of protein activity [13–16]. As mentioned above, one of the important conditions for FRET to occur is the overlap of the emission spectrum of the donor with the absorption spectrum of the acceptor. As a result of spectral overlap, the FRET signal is always contaminated by donor emission into the acceptor channel and by the excitation of acceptor molecules by the donor excitation wavelength (see Fig. 1). Both of these signals are termed spectral bleedthrough (SBT) signal into the FRET channel. In addition to SBT, the FRET signals in the acceptor channel also require correction for spectral sensitivity variations in donor and acceptor channels, autofluorescence, and detector and optical noise, which contaminate the FRET signal [6,17]. Quantum yields (QY) usually vary between donor and acceptor molecules and are also part of the equation; protein–dye conjugates also have considerably lower QYs compared to the pure dye.

There are various methods to assess the SBT contamination in FRET image acquisition. Donor spectral bleedthrough (DSBT) can be calculated and corrected using the percentage of the spectral area of the donor emission spill over into the acceptor emission spectrum or FRET channel (see Fig. 1). In the case of acceptor spectral bleedthrough (ASBT) it is difficult to determine the fraction of excitation of the acceptor by the donor wavelength and its emission in the acceptor channel. Moreover, there are methods available in the literature for FRET data analysis to correct for any variation in the expression or concentration of the fluorophore labeled to the cells [8,17,23]. Depending on the level of sensitivity desired, other methods use two or three filter sets to normalize the FRET signal for the donor [6] and acceptor [18] SBT signal. There are other approaches of SBT correction after image acquisition using single-label reference specimens [6,18–22]. Most of these algorithms are based on the assumption that the ratio of SBT and fluorescence intensity is constant, which we have called CR (constant ratio). In reality the ratio of SBT and fluorescence intensity is dependent on

different fluorescence intensity level as described in the literature ([17,23]; www.circusoft.com), named IR (intensity range based ratio). In our hands, the ratio is seldom constant, however, depending on the desired level of sensitivity, the CR approach may be adequate. On the other hand, sensitive contamination removal becomes very critical in the case of quantitation of the FRET signal or to calculate the distance between the interacting molecules.

In this paper we consider Gordon *et al*. [6] algorithm as an example of CR approach and Chen *et al*. [17] as an example for IR approach to show the differences between these two approaches in live cellular environments.

MATERIALS AND METHODS

Cell Preparation

CAATT/Enhancer Binding Protein Alpha (C/EBPα)

For the studies described here the sequence encoding the DNA binding and dimerization domain of the transcription factor C/EBPα [24] was fused in-frame to commercially available CFP or YFP color variants (www.clontech.com) to generate CFP-C/EBPα and YFP-C/EBPα [25]. Mouse pituitary GHFT1-5 cells were harvested and transfected with the indicated plasmid DNA(s) by electroporation [14]. The total input DNA was kept constant using empty vector DNA. Cell extracts from transfected cells were analyzed by Western blot to verify the tagged proteins were of the appropriate size as described previously. For imaging, the cells were inoculated dropwise onto a sterile cover glass in 35 mm culture dishes and allowed to attach prior to gently flooding the culture dish with media. They were maintained for 18–36 h prior to imaging. The cover glass with attached cells was inserted into a chamber containing the appropriate medium and the chamber was then placed on the microscope stage.

Polarized Epithelial Cells

Polarized epithelial MDCK cells, stably transfected with polymeric IgA receptor (pIgA-R), were grown for three days in Transwell-Clear inserts, washed with PBS and followed by internalization of 160 μg/ml pIgA-R-IgG ligands ($[Fab]_2$ pseudo ligands) conjugated to Alexa488 (www.probes.com) or Cy3 (www. Amersham.com) for four hours at 17°C. The ligands were applied to the apical and basolateral plasma membrane (PM), respectively. At 17°C the pIgA-R-ligand complexes moved into the subapical region [8,26]. Then, the cells were washed with PBS to remove unbound ligands and immediately fixed with 4% paraformaldehyde/PBS. We internalized the Alexa488- and Cy3-labeled ligands at a donor:acceptor ratio of 1:1. In all, three different samples were used: The double-labeled specimen, containing apically internalized Alexa488-pIgA-R-ligand (donor) complexes and basolaterally internalized Cy3-pIgA-R-ligand complexes (acceptor), plus corresponding reference samples containing either Alexa488 or Cy3 that were used to establish the spectral bleed-through levels (see below).

INSTRUMENTATION AND DATA ACQUISITION

Laser scanning confocal FRET (C-FRET) microscopy overcomes the limitation of out-of focus information owing to its capability of rejecting signals from outside the focal plane and acquire the signal in real-time [5–8,17,27]. This capability provides a significant improvement in lateral resolution and allows the use of serial optical sectioning of the living specimen. By selecting appropriate filter combinations one can configure any commercially available confocal microscopy system for FRET imaging [28] (www.chromatech.com; www.omegaoptical.com).

Data used in this paper were collected from three microscopy systems including wide-field [29], Nikon PCM2000 confocal [8,23] and Biorad Radiance2100 [30]. Here we explain briefly the Biorad Radiance2100 confocal microscopy system (www.zeiss.com). The system consists of a Nikon TE300 epifluorescent microscope with a 100 W Hg Arc Lamp. A Plan Fluor 60x NA 1.4 water objective lens was used for confocal FRET (C-FRET) image acquisition. TE300 was coupled to Biorad Radiance2100 confocal/multiphoton system. A 50 mW argon-ion laser (457, 488, and 514 nm), HeNe Green (543 nm), and a laser diode laser (633) was coupled to the laser port of a Radiance2100. The 457 and 514 nm laser line was used to acquire the dimerization of protein images of CFP and YFP expressed in GHFT1-5 cell nucleus. We have also used FRET images collected using the polarized cell labeled with Alexa488 and Cy3 with Nikon PCM2000 confocal microscope.

In brief, to remove the SBT or cross-talk contained in the C-FRET signal, images were acquired as listed in Table I: double-labeled (three images: donor excitation (donor and acceptor channels, acceptor excitation/acceptor channel), single-labeled donor (two images: donor excitation/donor and acceptor channels) and single-labeled acceptor (two images: donor excitation/acceptor channel; acceptor excitation/acceptor channel) with appropriate filters for FRET data analysis as described in the literature [6,8,17,23,28,30]. The SBT approach works on the assumption that the double-labeled cells and

Table I. Data Acquisition and the Respective Symbols Used for the Two Algorithms Described in this Paper

Symbol(Elangovan *et al*. [23] and Chen *et al*. [17])	Symbol (Gordon *et al*. [6])	Fluorophores	Excitation wavelength	Emission wavelength	Meaning
a	Dd	Donor	Donor	Donor	Signal from donor only specimen with donor excitation/donor emission
b	Fd	Donor	Donor	Acceptor	Signal from donor only specimen with donor excitation/acceptor emission
c	Fa	Acceptor	Donor	Acceptor	Signal from acceptor only specimen with donor excitation/acceptor emission
d	Aa	Acceptor	Acceptor	Acceptor	Signal from acceptor only specimen with acceptor excitation/acceptor emission
e	Df	Donor and acceptor	Donor	Donor	Signal from donor and acceptor specimen with donor excitation/donor emission
f	Ff	Donor and acceptor	Donor	Acceptor	Signal from donor and acceptor specimen with donor excitation/acceptor emission
g	Af	Donor and acceptor	Acceptor	Acceptor	Signal from donor and acceptor specimen with acceptor excitation/acceptor emission
h		Donor	Acceptor	Donor	Signal from donor only specimen with acceptor excitation/donor emission
i	Ad	Donor	Acceptor	Acceptor	Signal from donor only specimen with acceptor excitation/acceptor emission
j	Da	Acceptor	Donor	Donor	Signal from acceptor only specimen with donor excitation/donor emission
k		Donor and acceptor	Acceptor	Donor	Signal from donor and acceptor specimen with acceptor excitation/donor emission

single-labeled donor and acceptor cells, imaged under the same conditions, exhibit the same SBT dynamics. The hurdle we had to overcome was the fact that we had three different cells (D, A, and D+A), where individual pixel locations cannot be compared. What could be compared, however, were pixels with matching fluorescence levels (Table I: a/e & d/g). Our algorithm follows fluorescence levels pixel-by-pixel to establish the level of SBT in the single-labeled cells, and then applies these values as a correction factor to the appropriate matching pixels of the double-labeled cell.

To establish PFRET (Processed FRET), i.e. the-contamination-removed FRET signal the following equation is applied [17,23]

$$\text{PFRET} = u\text{FRET} - \text{DSBT} - \text{ASBT} \tag{1}$$

where *u*FRET is contaminated FRET (signal in the FRET/acceptor channel).

Conventionally, energy transfer efficiency (E) is calculated by ratioing the donor image in the presence (I_{DA}) and absence (I_D) of acceptor. To execute this calculation, the acceptor in the double-label specimen either has to be bleached or the donor fluorescence averages of two different cells (single and double label) with most likely different dynamics are used in the efficiency calculation. When using the algorithm as described, we indirectly obtained the I_D image by using the FRET image [23]. The sensitized emission in the acceptor channel is due to the quenching of the donor or energy transferred signal from the donor molecule in the presence of acceptor. Therefore, if we add the PFRET value back to the intensity of I_{DA}, pixel-by-pixel, we obtain I_D. Hence, the efficiency equation will be modified to obtain the new transfer efficiency (E_n) from the same cell which is shown in Eqs. (3) or (4)

$$E = 1 - \frac{I_{DA}}{I_D} \tag{2}$$

$$E_n = 1 - \frac{I_{DA}}{I_{DA} + \text{PFRET}} \tag{3}$$

or

$$E_n = \frac{\text{PFRET}}{I_{DA} + \text{PFRET}} \tag{4}$$

Where

$$I_D = I_{DA} + \text{PFRET} \tag{5}$$

The new efficiency (E_n) is calculated by generating a new I_D image by including the detector spectral sensitivity of donor and acceptor channel and the donor/acceptor quantum yields with FRET signal as shown in Eqs. (6) or

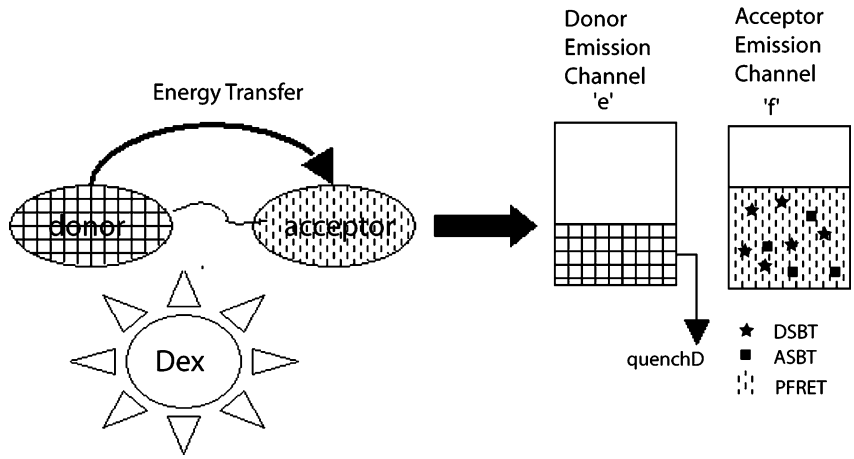

Fig. 2. Illustration of DSBT and ASBT signal distribution in the FRET channel. The doubly expressed (labeled) cell excited with donor excitation wavelength the energy is transferred nonradiatively to the acceptor molecules. The energy transfered signal (FRET) detected in the acceptor emission channel ('*f*') is contaminated with donor spectral bleedthrough (DSBT) and acceptor spectral bleedthrough (ASBT). '*e*' is the quenched donor image.

(7) [17].

$$E_{\mathrm{n}} = 1 - \frac{I_{\mathrm{DA}}}{I_{\mathrm{DA}} + \mathrm{PFRET} \times (\psi_{\mathrm{dd}}/\psi_{\mathrm{aa}}) Q_{\mathrm{d}}/Q_a} \tag{6}$$

Or the Eq. (6) can be rewritten as

$$E_{\mathrm{n}} = \frac{\mathrm{PFRET} \times SS \times QY}{(\mathrm{PFRET} \times SS \times QY) + I_{\mathrm{DA}}} \tag{7}$$

where

$$\begin{aligned} SS &= (\psi_{\mathrm{dd}}/\psi_{\mathrm{aa}}) \\ &= [(\text{PMT gain of donor channel}/\text{PMT gain of} \\ &\quad \text{acceptor channel})(\text{spectral sensitivity of donor} \\ &\quad \text{channel}/\text{spectral sensitivity of acceptor channel})] \\ QY &= Q_{\mathrm{d}}/Q_{\mathrm{a}} - Q_{\mathrm{d}}, \text{ and } Q_{\mathrm{a}} \text{ are donor and acceptor} \\ &\quad \text{quantum yield, respectively} \end{aligned} \tag{8}$$

In Eq. (9) for estimating the distance between donor and acceptor, r, has changed to r_{n}. Förster's distance R_0 value was calculated for various fluorophore pairs [17,23]

$$r = R_0 \left(\frac{1}{E} - 1 \right)^{1/6} \tag{9}$$

$$r_{\mathrm{n}} = R_0 \left(\frac{1}{E_{\mathrm{n}}} - 1 \right)^{1/6} \tag{10}$$

DATA ANALYSIS

As mentioned above, the major contaminations are the DSBT and ASBT which have to be removed by using control images. All optical conditions such as excitation power, gain of the photomultiplier tubes (PMT), and the pinhole size (iris) were kept the same to collect these seven images. As shown in the cartoon (Fig. 2) the FRET image '*f*' and the quenched donor image '*e*' (I_{DA}) were acquired by exciting the CFP-YFP-C/EBPα expressed in the living cell nucleus with donor excitation wavelength. The contaminated FRET image '*f*' contains the background noise, DSBT, ASBT and FRET signal. The background signal can be removed by using an image acquired under same optical conditions with no cells in the filed of view or using unlabeled cells. Then, the donor bleedthrough ratio r_d was estimated by acquiring the donor only signal image '*a*' and the donor bleedthrough image '*b*' using the singly expressed cell CFP-C/EBPα by exciting with donor excitation wavelength. Then, the DSBT was estimated using the following equations

$$r_d = \frac{b}{a} \tag{11}$$

$$\mathrm{DSBT} = e r_d \tag{12}$$

The ASBT added to the '*f*' image due to the excitation of the acceptor molecule by the donor excitation wavelength (see Fig. 1). In order to remove the ASBT contamination in '*f*' an acceptor alone expressed cell (YFP-C/EBPα) was subjected to donor and acceptor excitation wavelengths to

collect the acceptor channel image '*c*' and '*d*' respectively (see Table I). As a reference an image '*g*' was collected from the doubly expressed cell by excitation with the acceptor wavelength (see Table I). These images were used to estimate the ASBT bleedthrough ratio r_a in '*f*' image.

$$r_a = \frac{c}{d} \tag{13}$$

$$\text{ASBT} = g r_a \tag{14}$$

Then, the PFRET signal in '*f*' was estimated using the Equation (1). If we replace DSBT and ASBT in Eq. (1) using Eqs. (11–14),

$$\text{PFRET} = u\text{FRET} - eb/a - gc/d \tag{15}$$

where uFRET is image '*f*'.

Equation (15) is equivalent to the Eq. (8b) as outlined in Gordon *et al*. [6] if *G* is equal to one, and Da and Ad is equal to zero by using appropriate filters,.

In the case of CR, in Eq. (15) the DSBT ratio is *b*/*a*, and the ASBT ratio is *c*/*d*. On the other hand, the IR approach uses the intensity range based SBT ratio estimation and is derived from Eqs. (11–14) are listed below, [17].

$$r_{d(j)} = \frac{\sum_{i=1}^{i=m} b_i}{\sum_{i=1}^{i=m} a_i} \tag{16}$$

$$\text{DSBT}_{(j)} = \sum_{p=1}^{p=n} (e_p r_{d(j)}) \tag{17}$$

$$\text{DSBT} = \sum_{j=1}^{j=k} \text{DSBT}_{(j)} \tag{18}$$

$$r_{a(j)} = \frac{\sum_{i=1}^{i=m} c_i}{\sum_{i=1}^{i=m} d_i} \tag{19}$$

$$\text{ASBT}_{(j)} = \sum_{p=1}^{p=n} (g_p r_{a(j)}) \tag{20}$$

$$\text{ASBT} = \sum_{j=1}^{j=k} \text{ASBT}_{(j)} \tag{21}$$

where *j* is the *j*th range of intensity, $r_{d(j)}$ and $r_{a(j)}$ are the donor and acceptor bleedthrough ratios for the *j*th intensity range, m is the number of pixel in '*a*' and '*d*' for the *j*th range, a_i and d_i are the intensities of pixel *i*, $\text{DSBT}_{(j)}$ and $\text{ASBT}_{(j)}$ are the donor and acceptor bleedthrough factors for the range *j*, *n* is the number of pixel in '*e*' and '*g*' for the *j*th range, $e_{(p)}$ and g_p are the intensity of pixel (*p*), *k* and *l* are the number of range and DSBT and ASBT are the total donor and acceptor SBTs respectively. (see Table I)

RESULTS AND DISCUSSION

The variation in detector sensitivity of a system plays a major role in the value of the SBT ratio and establishing that factor is important to obtain the true estimation of the rate of energy transfer efficiency (*E*%). Here we describe two system configurations one with CCD camera used in the wide-field FRET (W-FRET) microscopy [28–29] and another one with PMT used in the confocal FRET (C-FRET) microscopy [8,23,30] systems. From the Eqs. (12, 14, 17, and (20), it demonstrates that its important to estimate correctly the SBT ratio r_a and r_d. Over- or underestimation of the SBT ratio will lead to error in calculating DSBT and ASBT. Further, it affects *E*% and introduces errors in the interpretation of the data for various biological situations.

IR (Intensity Range Based) Versus CR (Constant Ratio)

In Fig. 3A and B, the plot of DSBT ratio r_d was plotted using the same cell line (CFP-C/EBPα protein (donor alone) expressed in GHFT1-5 cell nucleus) for different (wide-field and confocal) FRET microscope system. In Fig. 3A the wide-field FRET microscope produces same SBT ratio for both IR and CR methodology which means SBT ratio is independent of fluorescence intensity level. This could be attributed to the camera quantum efficiency which is almost constant in the visible spectrum (www.hamamatsuphotonics.com). On the other hand the C-FRET microscope system (Fig. 3B) produces a non-constant SBT ratio for IR, particularly at the low intensity levels it has a higher ratio than that at the higher intensity level. This could be attributed to the response of the spectral sensitivity of the PMT. Therefore, if we use CR to correct SBT in the confocal system (Biorad Radiance2100), we may overestimate the SBT which will affect *E*%. As an example, CR is a fixed 0.24 (Fig. 3B), compared with the varying levels in IR. Depending on different fluorescent intensity level, the CR is higher than IR. In this case the CR and IR methodology will provide different DSBT and ASBT, resulting in different PFRET and *E*% values.

Now we compare different confocal systems (Biorad Radiance2100, Fig. 3C and Nikon PCM2000, Fig. 3D) to estimate the SBT ratio for Alex488-pIgA-R-ligand (donor alone) in polarized epithelial MDCK cells [8]. In Fig. 3C, at most intensity levels, the ratio is constant except at the level 1–2. As shown in Fig. 3C very high b/a ratio 0.36 was obtained using CR and this over estimation of SBT provides very low *E*% value. To avoid overestimating SBT by using CR, we can set up threshold values to

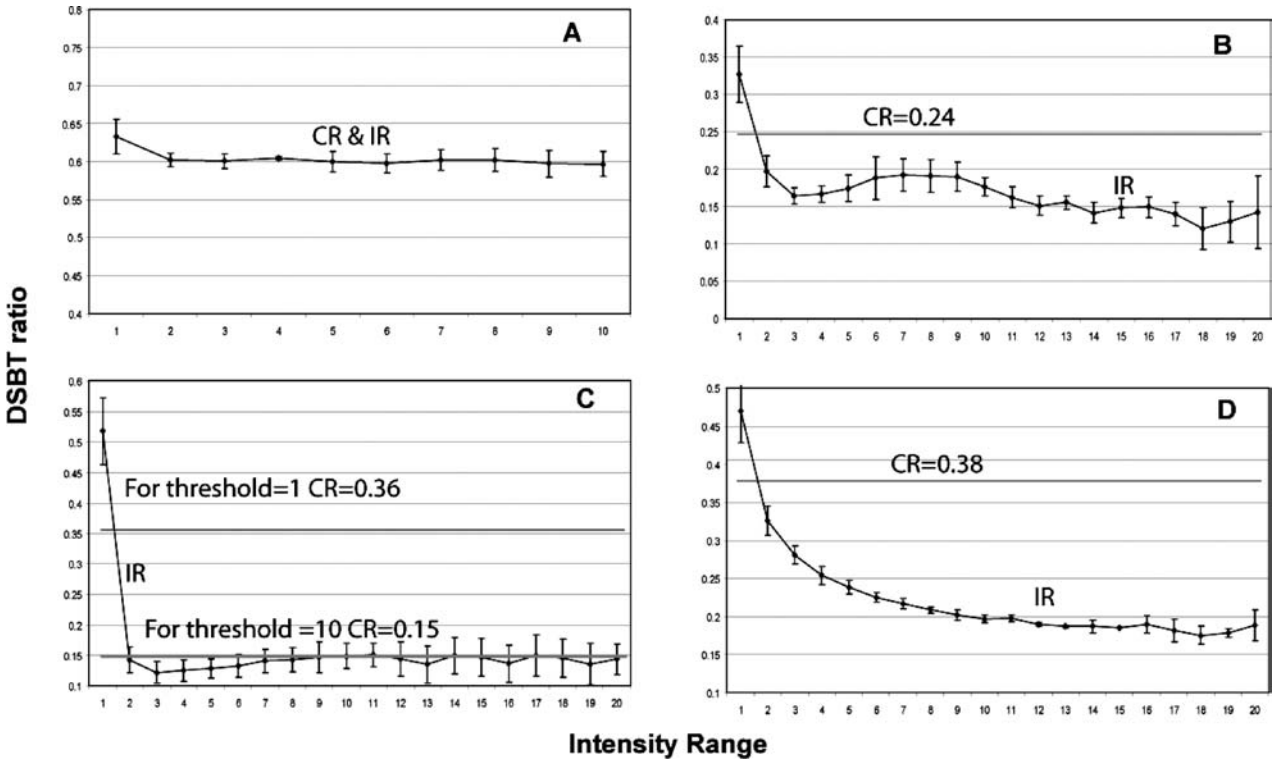

Fig. 3. Comparison of intensity range based SBT ratio (IR) and constant SBT ratio (CR) for different microscopy systems and for different cell lines. By way of example, we have demonstrated only for the DSBT and the ASBT also shows the same pattern (not shown). (A) CFP-C/EBPα (donor alone) expressed in GHFT1-5 cell nucleus was used to obtain the images '*a*' and '*b*' in the wide-field FRET microscopy system to estimate the CR and IR DSBT ratio. As shown in the figure this is constant in both cases. (B) The same cell was used in the Biorad Radiance2100 confocal microscopy system. The IR ratio is not uniform and a steady fall between the intensity levels of 1 and 2 but it provides stable *E%* estimation. On the other hand the CR expected to give less *E%* value compared to CR since the ratio value is higher than the IR. The low level variation in IR did not affect the estimation of the *E%* value. (C & D) Alex488-pIgA-R-ligand (donor alone) in polarized epithelial MDCK cells was used in both Nikon PCM2000 and Biorad Radiance2100 confocal microscopy systems. As noticed in the figures, CR and IR have different distributions of the DSBT ratio. In (C) different threshold setting provide different DSBT ratio value which affects the *E%* calculation. In (D), it is difficult to set the threshold value in IR since the change in DSBT ratio decreases smoothly with increasing fluorescence intensity. On the other hand, IR does not require any threshold setting to obtain a stable *E%* estimate to calculate the distance between interacting molecules. (see the text for more details).

exclude the first intensity level to make the CR close to the IR in most intensity level. In this case the threshold value is 10. Setting up threshold value can solve the problem of overestimating SBT with CR under one condition that threshold value should not be too high to lose useful information in the excluded pixels. However in the case of Fig. 3D, setting up threshold value to get CR is not right way because the ratio decreases smoothly with the increase in fluorescence intensity level. It is difficult to find a threshold value for CR close to IR for all the intensity level without losing the true signal. In this kind of situation IR is the appropriate methodology to use to estimate the SBT ratio.

Why may CR cause overestimation of SBT? As shown in Fig. 3B and 3C, the ratio significantly decreased from intensity level 1 to level 2. When calculating CR, we use the mean ratio of pixels, since the number of low level (level 1) intensity pixels may dominate the total number of pixels, it results in higher ratio of the mean value of all pixels. In some case, the low-level intensity pixels do not have much true information except noise or background. So we can set up threshold value to exclude those factors without losing true information. However, IR calculates ratios for different intensity levels, the high ratios at low intensity levels only affect those areas, which we believe to be mostly noise or background, but importantly, it does not affect the true signal area. In the case of IR, there is no need to set up a threshold value.

As an example in Fig. 4, we used both CR and IR methodology to remove the DSBT contamination. The CR provides more DSBT values (DSBTii) than the IR (DSBTi). IR was put through a rigorous test by examining different ranges of intensity (Fig. 4, table insert). For CR, mean intensity was ratioed to obtain a constant value

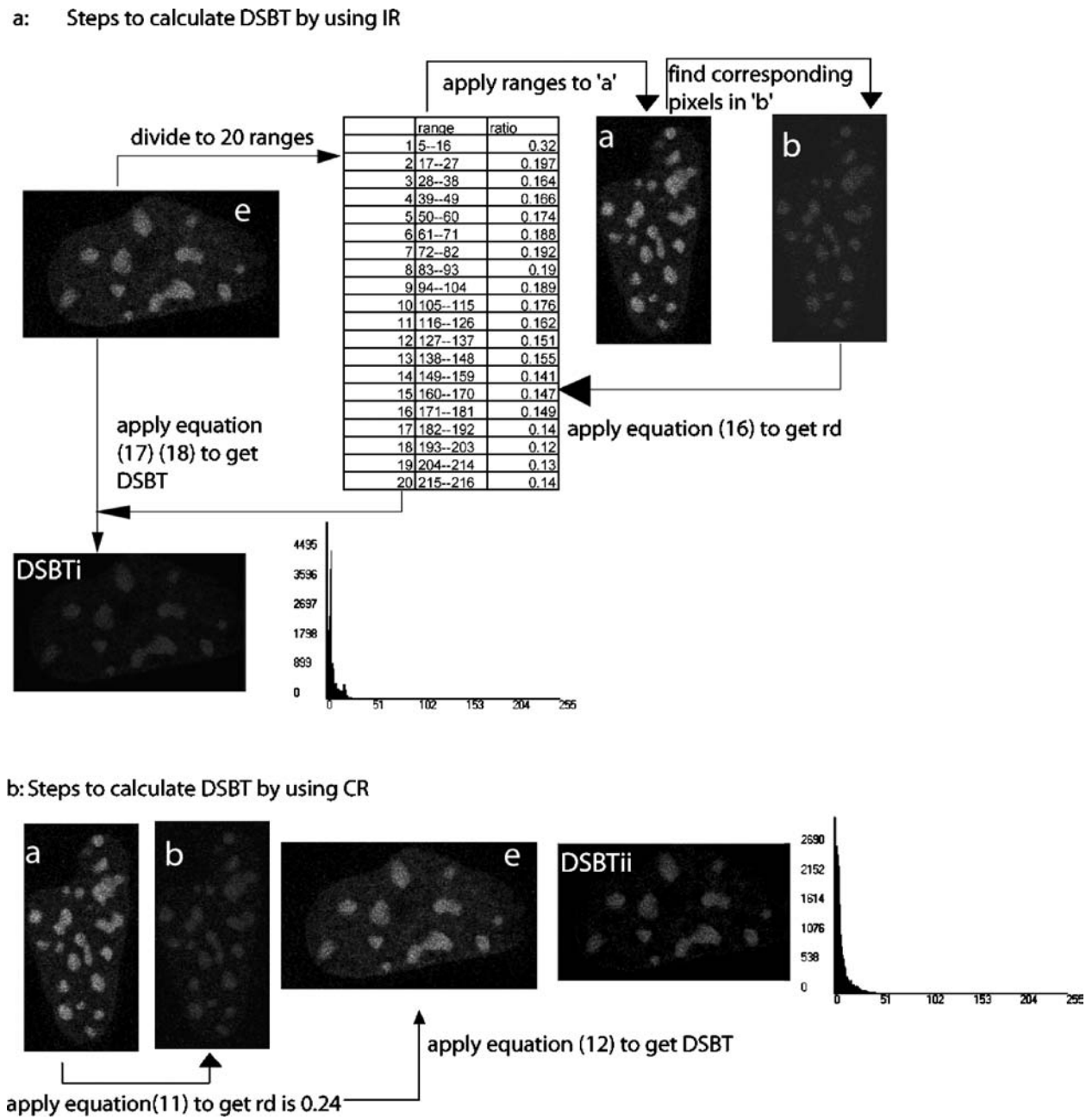

Fig. 4. Demonstrate the difference for estimation of DSBT ratio for the CFP-C/EBPα (donor alone) expressed in GHFT1-5 cell nucleus by using CR and IR. In the case of IR, the gray level intensity distribution in image '*e*' was 5-216 and was divided into 20 intensity ranges as shown in the table insert. These intensity ranges were applied in image '*a*' and the corresponding SBT pixels were identified in '*b*'. Using Eqs. (16–18) the DSBT were estimated as shown in DSBTi. In the case of CR, the mean intensity value of the image '*a*' and '*b*' were used in Eq. (11) to estimate the bleedthrough ratio and then the DSBT was calculated using Eq. (12) and the result shown in DSBTii. This clearly demonstrates that the CR methodology provides higher DSBT value compared to IR as shown in their respective histograms.

of 0.24 and was used as DSBT value for bleedthrough correction. *E%* is higher for the IR than for the CR approach, resulting in a difference of 8–10% in absolute *E%* between these two approaches. The CR approach may cause overestimation of SBT in most situations and therefore, reduce the *E%* value. This difference in the absolute value of *E%* becomes critical for distance *r* estimates and is generally important for quantitative interpretation of data. The

Table II. Compare Constant Ratio and Intensity Range Based Ratio

	Constant ratio Equations (11) and (13)	Intensity range based ratio Equations (16) and (19)
Advantage	Easy to understand, easy to use. No need to use special software, because, it only needs functions like ratio image, multiply constant value to an image, and subtract image which are available in most commercial imaging software	Corrects different SBT ratio due to different fluorescence intensity level, avoid over- or under- estimation of SBT ratio. Suitable for any FRET microscopy systems or cell lines
Disadvantage	It is good for Wide-Field FRET Microscopy, but for confocal or multiphoton FRET microscopy, it requires more attention to calibrate the SBT ratio by choosing area and setting up appropriate threshold values to reduce the influence of background and noise signal in the estimation of SBT	Need special software (PFRET, www.circusoft.com). or anyone can write their own code to implement the algorithm to estimate the SBT ratio

advantages and disadvantages of CR and IR methodology are shown in Table II.

Different algorithms were compared by Barney and Danuser [31] and concluded that Gordon *et al*. [6] algorithm was able to detect the lower level FRET signal. This is possible by selecting appropriate threshold level. On the other hand, threshold is not required in Chen *et al*.[17] and also provide stable results in the E% calculation. Gordon *et al*. [6] discuss that there is a possibility of back bleedthrough of FRET signal in the quenched donor channel in the image '*e*' (FRET_Back) and so the image '*e*' could have been contaminated. In our opinion this is not possible since maximum FRET occurs at the peak absorption and peak emission [32]. Also, we do not expect any occurrence of FRET by the acceptor excitation wavelength (FRET_g) in most confocal systems. But it may happen in two-photon system. Moreover, it may be possible that there may be some back-bleedthrough of ASBT signal in the quenched donor channel (ASBT_Back) and donor bleedthorugh while exciting the double labeled cell with acceptor excitation wavelength (DSBT_g) in the case of two-photon excitation FRET microscopy and we were able to observe such occurrences [17] for selected excitation average power at the specimen plane. In general, in our observation these unconventional bleedthrough components were very minimal (within noise level) or negligible in any FRET microscopy systems [17]. These types of bleedthrough may be become a factor if one uses higher average power at the specimen plane as in the case of two-photon FRET microscopy system [17].

Table III. Comparison of SBT Correction in Two-Different Algorithm

Reference	Gordon *et al*. [6]	Chen *et al*. [17]
SBT ratio	Constant ratio	Intensity range based ratio
Number of bleedthrough corrected	1. DSBT 2. ASBT 3. ASBT_Back 4. DSBT_g 5. FRET_g 6. FRET_Back	1. DSBT 2. ASBT 3. ASBT_Back 4. DSBT_g 5. No 6. No
Spectral sensitivity correction	Yes	Yes
Images	9	11
Software	Integrated into some commercial system	Stand alone PFRET Software, available with Circusoft.com

We would like to mention that by using proper filter sets and excitation power, cross talk 3, 4, 5, 6 (see Table III) can be considerably reduced or negligible. In this case, the difference between Gordon *et al*. [6] and Chen *et al*. [17] is only the SBT ratio estimation. Both algorithms require only the first 7 images listed in Table I to estimate the SBT ratio.

CONCLUSION

Both Chen *et al*. [17] and Gordon *et al*. [6] algorithms were described to estimate the SBT ratio and its influence in the estimation of the bleedthorugh ratio and impact on the rate of energy transfer efficiency. Both techniques are equally useful to remove the SBT contamination in the FRET signal but the Chen *et al*. [17] technique does not require a threshold approximation in estimating the SBT ratio. Each algorithm was developed to sort out some of the difficulties faced by the researchers in their investigations. In general, these subtle differences between algorithms may or may not affect the efficiency or distance estimation. The investigators should decide which algorithm methodology or the FRET microscopy system is suitable for their biological investigations.

ACKNOWLEDGMENTS

We wish to acknowledge the funding provided by the National Center for Research Resources (NCRR-NIH,

RR021202) and the University of Virginia. We also wish to thank Drs. Margarida Barroso, Richard Day and Horst Wallrabe for their valuable suggestions.

REFERENCES

1. R. M. Clegg (1996). In X. F. Wang and B. Herman (Eds.), *Fluorescence Imaging Spectroscopy and Microscopy*, Wiley, New York, pp. 179–251.
2. T. Förster (1948). Intermolecular energy migration and fluorescence. *Ann. Phys. (Leipzig)* **2**, 55–75.
3. L. Stryer (1978). Fluorescence energy transfer as a spectroscopic ruler. *Annu. Rev. Biochem.* **47**, 819–846.
4. E. A. Jares-Erijman and T.M. Jovin (2003). FRET imaging. *Nat. Biotechnol.* **21**(11), 1387–1395.
5. B. A. Cunningham (2001). Finding a mate. *The Scientist* **15**, 7–26.
6. G. W. Gordon, G. Berry, X. H. Liang, B. Levine, and B. Herman (1998). Quantitative fluorescence resonance energy transfer measurements using fluorescence microscopy. *Biophys. J.* **74**, 2702–2713.
7. A. Periasamy and R. N. Day (2005). *Molecular Imaging: FRET Microscopy and Spectroscopy*. Oxford University Press: New York.
8. H. Wallrabe, M. Elangovan, A. Burchard, A. Periasamy, and M. Barroso (2003). Confocal FRET microscopy to measure clustering of receptor-ligand complexes in endocytic membranes. *Biophys. J.* **85**, 559–571.
9. H. Wallrabe and A. Periasamy (2005). FRET-FLIM microscopy and spectroscopy in the biomedical sciences. *Curr. Opin. Biotech.* **16**, 19–27.
10. A. Hoppe, K. A. Christensen, and J. A. Swanson (2002). Fluorescence resonance energy transfer-based stoichiometry in living cells. *Biophys. J.* **83**, 3652–3664.
11. J. R. Lakowicz (1999). *Principles of Fluorescence Spectroscopy*, 2nd ed., Plenum Press, New York.
12. A. Periasamy (2001). *Methods in Cellular Imaging*, Oxford University Press, New York.
13. A. B. Cubitt, R. Heim, S. R. Adams, A. E. Boyd, L. A. Gross, and R. Y. Tsien (1999). Understanding, improving and using green fluorescent proteins. *Trends Biochem. Sci.* **20**, 448–455.
14. R. N. Day (1998). Visualization of Pit-1 transcription factor interactions in the living cell nucleus by fluorescence resonance energy transfer microscopy. *Mol. Endo.* **12**, 1410–1419.
15. J. Lippincott-Schwartz and G. H. Patterson (2003). Development and use of fluorescent protein markers in living cells. *Science* **300**(5616), 87–91.
16. A. Miyawaki and R. Y. Tsien (2000). Monitoring protein conformations and interactions by fluorescence resonance energy transfer between mutants of green fluorescent protein. *Methods Enzymol.* **327**, 472–500.
17. Y. Chen, M. Elangovan, and A. Periasamy (2005). In A. Periasamy and R. N. Day (Eds.), *Molecular Imaging: FRET Microscopy and Spectroscopy*, Oxford University Press, New York, pp. 126–145.
18. Z. Xia and Y. Liu (2001). Reliable and global measurement of fluorescence resonance energy transfer using fluorescence microscopes. *Biophys. J.* **81**, 2395–2402.
19. V. S. Kraynov, C. Chamberlain, G. M. Bokoch, M. A. Schwartz, S. Slabaugh, and K. M. Hahn (2000). Localized Rac activation dynamics visualized in living cells. *Science* **290**, 333–337.
20. L. Tron, J. Szollosi, S. Damjanovich, S. Helliwell, D. Arndt-Jovin, and T. Jovin (1984). Flow cytometric measurement of fluorescence resonance energy transfer on cell surfaces. Quantitative evaluation of the transfer efficiency on a cell-by-cell basis. *Biophys. J.* **45**, 939–946.
21. F. S. Wouters, P. I. Bastiaens, K. W. Wirtz, and T. M. Jovin (1998). FRET Microscopy demonstrates molecular association of non-specific lipid transfer protein (nsL-TP) with fatty acid oxidation enzymes in peroxisomes. *Embo. J.* **17**, 7179–7189.
22. D. C. Youvan, C. M. Silva, E. J. Bylina, W. J. Coleman, M. R. Dilworth, and M. M. Yang (1997). Calibration of fluorescence resonance energy transfer in microscopy using genetically engineered GFP derivatives on nickel chelating beads. *Biotechnol. et alia* **3**, 1–18.
23. M. Elangovan, H. Wallrabe, Y. Chen, R. N. Day, M. Barroso, and A. Periasamy (2003). Characterization of one- and two-photon excitation resonance energy transfer microscopy. *Methods* **29**, 58–73.
24. D. Lew, H. Brady, K. Klausing, K. Yaginuma, L. E. Theill, C. Stauber, M. Karin, and P. Mellon (1992). GHF-1-promoter-targeted immortalization of a somatotropic progenitor cell results in dwarfism in transgenic mice. *Genes Dev.* **7**, 683–693.
25. A. J. Lincoln, C. Williams, and P. F. Johnson (1994). A revised sequence of the rat c/ebp gene. *Genes Dev.* **8**, 1131–1132.
26. M. Barroso and E. S. Sztul (1994). Basolateral to apical transcytosis in polarized cells is indirect and involves BFA and trimeric G protein sensitive passage through the apical endosome. *J. Cell Biol.* **124**, 83–100.
27. A. K. Kenworthy, N. Petranova, and M. Edidin (2000). High-resolution FRET microscopy of cholera toxin B-subunit and GPI-anchored proteins in cell plasma membranes. *Mol. Biol. Cell* **11**, 1645–1655.
28. R. B. Sekar and A. Periasamy (2003). Fluorescence resonance energy transfer (FRET) microscopy imaging of live protein localization. *J. Cell Biol.* **160**, 629–633.
29. A. Periasamy, and R. N. Day (1999). Visualizing protein interactions in living cells using digitized GFP imaging and FRET microscopy. *Meth. Cell Biol.* **58**, 293–314.
30. J. D. Mills, J. R. Stone, J. D. Rubin, D. E. Melon, D. O. Okonkwo, A. Periasamy, and G. A. Helm (2003). Illuminating protein interactions in tissue using confocal and two-photon excitation fluorescent resonance energy transfer (FRET) microscopy. *J. Biomed. Opt.* **8**, 347–356.
31. C. Barney and G. Danuser (2003). FRET or no FRET: A quantitative comparison. *Biophys. J.* **84**, 3992–4010.
32. B. Herman, G. Gordon, N. Mahajan, and V. Centonze (2001). In A. Periasamy (Ed.), *Methods in Cellular Imaging*, Oxford University Press, New York, pp. 257–272.